Flow behavior and processing map of forging commercial purity titanium powder compact

Xiaoyan Xu[a)] and Yuanfei Han
State Key Laboratory of Metal Matrix Composites, Shanghai Jiao Tong University, Shanghai 200240, China

Changfu Li and Philip Nash
Mechanical, Materials & Aerospace Engineering, Thermal Processing Technology Center, Illinois Institute of Technology, Chicago, Illinois 60616, USA

Damien Mangabhai
Research and Development, Cristal Metal Inc., Lockport, Illinois 60441, USA

Weijie Lu
State Key Laboratory of Metal Matrix Composites, Shanghai Jiao Tong University, Shanghai 200240, China

(Received 18 December 2014; accepted 13 March 2015)

The flow behavior of forged commercial purity (CP) titanium powder compact was studied by developing a processing map. CP titanium powder was sintered to 94% relative density, then hot compressed in a Gleeble thermal–mechanical simulator at strain rates ranging from 0.001 to 10 s^{-1} and deformation temperatures ranging from 600 to 800 °C. The hot forging process improved the densification to 98–99.9% and reduced the grain size from 93 to 10 μm by the occurrence of dynamic recrystallization. The fully dynamic recrystallization region is in the range of deformation temperature of 750–800 °C and strain rate of 0.001–0.01 s^{-1}, with a power dissipation efficiency higher than 40%, determined by constructing a processing map and analyzing the volume fraction of dynamic recrystallization. This research provides a guide for powder compact forging of power metallurgy titanium by providing the hot compression parameters, which can lead to an improved microstructure and densification.

I. INTRODUCTION

Titanium and titanium alloys have a high strength to weight ratio and good corrosion resistance compared with stainless steel but require longer times and higher cost for machining.[1] Power metallurgy (PM) offers a viable approach to produce near net shape complex components with little if any machining.[2] The traditional PM technology includes powder fabrication, powder compaction, and sintering. Post sintering processes may be needed if better mechanical properties for the components are required. Sintering alone does not provide full density for the commercial purity (CP) titanium powder because gas is trapped inside the compact and the removal of small porosity depends on volume diffusion. The traditional press and sinter technology for fabricating Ti components usually achieves 92–95% relative density.[3,4] Hot isostatic pressing (HIP) and powder compact forging both can provide full density by eliminating the trapped gas in the compact. However, HIP rarely refines the microstructure of the components due to a small amount of energy provided. Powder forging combines the traditional PM method with the forging process, which can provide refined microstructure by dynamic recrystallization and densify the porous metal.[5] Zhang[4] reveals the relationship of relative density with the amount of deformation by simulating Ti–6Al–4V powder compact forging process using three dimension-finite element modeling (3D-FEM). That research shows that the relative density has a relationship with the deformation degree. The microstructure and the flow behavior of titanium alloy are very sensitive to the hot processing parameters.[6] By using the approach of developing a processing map, which is widely used to design hot working parameters, the characterization of the forging behavior can be obtained. The processing map developed by Prasad et al.[7] consists of a superimposition of a power dissipation map and an instability map, which can indicate the stable and unstable domains during the metal deformation. Research has been done on processing maps for hot working titanium alloys,[8] which also emphasizes the influence of oxygen content during titanium deformation. The instability of the flow behavior of titanium alloy was studied by constructing a processing map and observation of the deformed microstructure.[9] Constitutive behavior of titanium and titanium alloys with microstructure evolution was also studied during the hot deformation process.[6,10–14] However, there is little

Contributing Editor: Jürgen Eckert
[a)]Address all correspondence to this author.
e-mail: xuxiaoyan727@hotmail.com, xuxiaoyan727@sjtu.edu.cn
DOI: 10.1557/jmr.2015.84

 © Materials Research Society 2015

https://doi.org/10.1557/jmr.2015.84 Published online by Cambridge University Press

research on the powder forging flow behavior analysis with most research focusing on bulk material. Jia et al.[15] studied the hot deformation behavior, dynamic recrystallization, and the nucleation mechanism of a powder metallurgy Ti–22Al–25Nb alloy without developing a processing map. In this work, we focus on constructing a forging processing map for CP Ti powder metallurgy components to establish how forging can improve consolidation and microstructure.

II. EXPERIMENTAL PROCEDURE

A. Sintering process

HDH CP Ti powder (product via the hydrogenation–dehydrogenation process) used in this work contains 0.206 wt% oxygen, 0.009 wt% nitrogen, 0.015 wt% hydrogen, 0.005 wt% carbon, and 0.025 wt% Fe. The particle size distribution is: 66% particles in the range of 75–150 μm, 32% particles in the range of 75–45 μm, and 2% below 45 μm. Powder was pressed at 690 MPa in double action die with a die wall lubrication and then sintered at 1370 °C (2500 °F) for 90 min in a 10^{-6} Torr vacuum furnace with a heating rate of 20 °C min^{-1}, followed by a furnace cool. The sintered compacts were around 32 mm in length with 13 mm in wide and 7.6 mm in thick. Sintered samples yield an average relative density of 94% measured by Archimedes' method based on MPIF Standard 42.[16] Oxygen, nitrogen, and carbon were measured on the sintered compact by a Leco TCH600 and Leco C230L based on ASTM:E1409 and ASTM:E1941.

B. Hot compression test

Sintered samples were sectioned into three equal pieces (10 mm in length, 4 mm in wide, and 2.5 mm in thick) with a diamond saw. The sectioned samples were placed into the Gleeble 3500 thermal simulator chamber (Dynamic Systems Inc., Poestenkill, NY), vacuumed to 10^{-7} Torr, and then heated up to target temperatures ranging from 600 to 800 °C, at intervals of 50 °C. Then the samples were forged at the target temperatures using strain rates from 10, 1, 0.1, 0.01 to 0.001 s^{-1} by 60% reduction. Tantalum foil was used to insulate the titanium compact from the compression anvils to minimize the friction and diffusion between them. After hot deformation process, the samples were cooled in the chamber within 2 min under vacuum.

C. Microstructure

The hot deformed samples were sectioned from the center line perpendicular to the press direction. Sectioned samples were mounted, ground, polished to 0.25 μm, and then etched with Kroll's etchant. The metallography of the sample center was observed using optical microscopy. Porosity and grain size for the fully dynamically recrystallized samples were measured using commercial ImageJ software. The volume fraction of the recrystallized grains was also quantitatively analyzed for the partially recrystallized sample.

III. RESULTS

A. Powder preform

Figure 1 shows the original microstructure of the sintered CP Ti compact hot deformed in the Gleeble tests to simulate the open die forge process. It can be seen that most of the pores are rounded and well distributed. The relative density is 94% with an average grain size of 93 μm, which is the typical grain size for the sintered HDH CP Ti powder compact. Small rounded pores indicated by yellow arrows are seated within the grains, which are not from the original HDH powder. A portion of the internal pores is from separation of pores and boundaries. Svoboda and Riedel[17] present that pores with a high mobility follow the migrating grain boundary easily, while those with a low mobility detach from the boundary. Kang[18] suggests a region of pore–grain boundary separation based on the sintering mechanisms. The sintered sample used in this work (94% relative density and 93 μm grain size) is highly possible in the range of "separation" with a reasonable extension of the trajectory. Another possible source of the shallow and small pores is the formation of etch pits which were highly suspected to be introduced during the etching process. This phenomenon is also shown in the sintering of prealloyed Ti–6Al–4V powder.[19] After sintering, the oxygen content increased from 0.206 to 0.25 wt% with C, N, H, and Fe showing little change.

B. Flow stress–strain curves

Figure 2 shows the true strain–stress curves on hot compression of the sintered CP Ti samples at different temperatures with different strain rates up to a 60% reduction. When the powder compact was hot compressed by

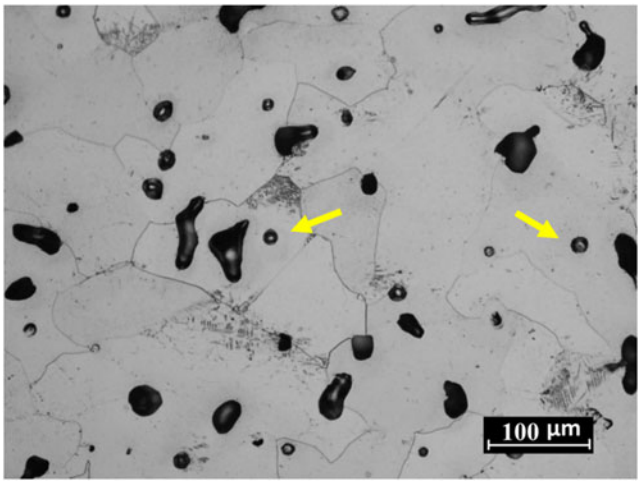


FIG. 1. CP Ti powder compact sintered at 1370 °C for 30 min with a sintered density of 94% and an average grain size of 93 μm.

https://doi.org/10.1557/jmr.2015.84 Published online by Cambridge University Press

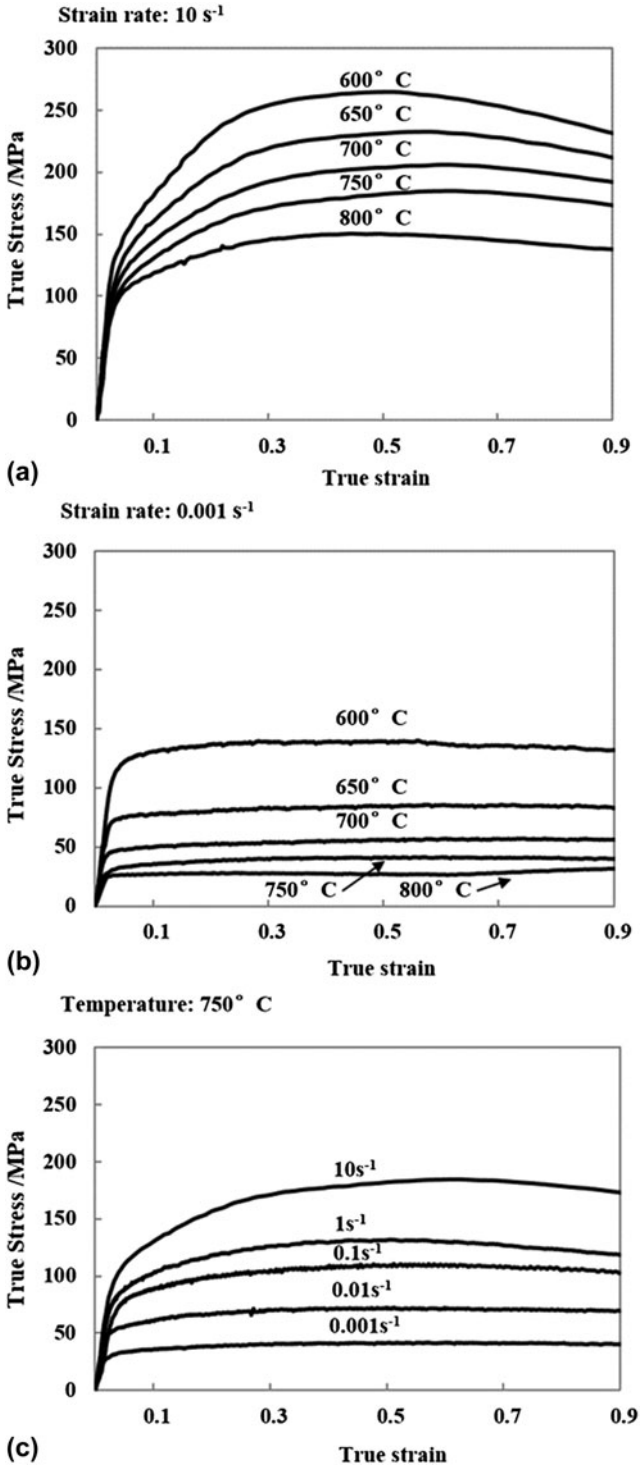


FIG. 2. True stress–true strain curves on forging the CP Ti sintered compacts by 60% reduction at: (a) 10 s^{-1} strain rate at different temperatures; (b) 0.001 s^{-1} strain rate; and (c) 750 °C at different strain rates.

10 s^{-1} strain rate in Fig. 2(a), with increasing the deformation temperature from 600 to 800 °C, the flow stress decreases from 270 to 150 MPa. The same phenomenon is observed in Fig. 2(b), which has a strain rate of 0.001 s^{-1}, the stable flow stress ranges from 140 to 25 MPa with increasing deformation temperature. These two figures indicate when the sample is hot deformed at the same temperature, a higher strain rate yields a higher flow stress as expected. The stress–strain curve at 600 °C shows a raise then a decline in Fig. 2(a), however, the stress–strain curves are getting smooth when deformation temperature goes up. One of the possible reasons is when material is deformed at a higher temperature, dynamic recrystallization balances the strain hardening which results in a plateau after the material reaches the yield point. While at a lower temperature (600 °C), metal strain hardening takes place without the compensation of dynamic recrystallization at a higher strain rate (10 s^{-1}), when the energy accumulated enough to initiate the recrystallization, the metal starts getting soft and the stress–strain curve declines [Fig. 2(a)]. Figure 2(c) shows that the strain rate has a proportional relationship with stable flow stress when the sample is deformed at 750 °C.

Figure 3 shows the etched microstructures of CP Ti sintered samples forged at 600 and 650 °C at 10 s^{-1} strain rate and 60% reduction. The porosities of the forged samples in Fig. 3 are obviously less than the porosity of the as sintered sample in Fig. 1. Some porosity does exist after hot forging, as indicated in Fig. 3(a). It also can be seen that there is a large amount of grain nucleation occurred along the deformed α grains and also in some preferred regions. There are some larger pores elongated in the hot deformed sample shown in Fig. 3(b).

IV. DISCUSSION

Hot powder forging can refine the grain size and also improve the densification of the powder metallurgy components. The constitutive equation for the CP Ti powder compact forging process can be established based on the flow stress–strain relationship. Based on the microstructure and the deformation processing map, the best processing parameters for CP Ti powder sintered components can then be determined.

A. Constitutive equation

There is a relationship between flow stress, deformation temperature, and strain rate when a metal is deformed at elevated temperatures. The flow behavior was described by Sellers and McTegart[20] as follows and the kinetic equation can be used to model the deformation response in the hot working process:

$$\dot{\varepsilon} = A[\sinh(\alpha\sigma)]^n \exp\left(-\frac{Q}{RT}\right) \quad , \qquad (1)$$

Where $\dot{\varepsilon}$ is the strain rate (s^{-1}), σ is the flow stress (MPa), n is the strain hardening exponent, and A, n, and α are the constants independent of the deformation temperature. Q is the deformation activation energy

https://doi.org/10.1557/jmr.2015.84 Published online by Cambridge University Press

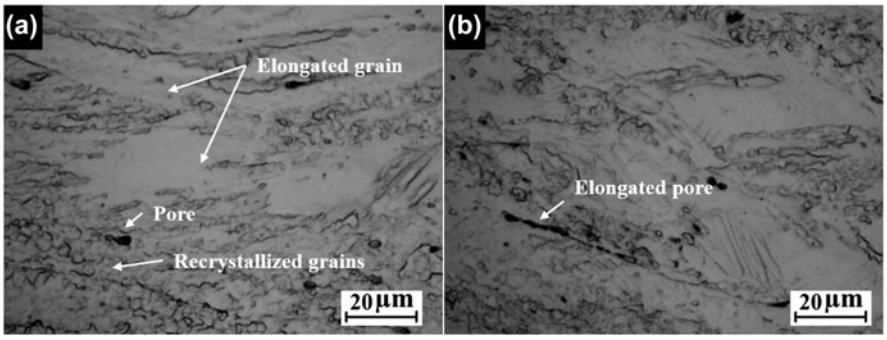


FIG. 3. Etched microstructures for forged CP Ti sintered components at 10 s^{-1} strain rate by 60% reduction at different temperatures: (a) 600 °C and (b) 650 °C.

(kJ mol^{-1}), R is the gas constant (kJ mol^{-1} K^{-1}), and T is the absolute temperature (K). This relationship reveals a direct proportional relationship between flow stress and strain rate, which confirmed by Fig. 2(c), and an inverse proportional relationship between flow stress and deformation temperature confirmed by Figs. 2(a) and 2(b).

According to Zener and Hollomon,[21] the flow stress and strain relationship can be represented by the parameter Z:

$$Z = \dot{\varepsilon}\exp\left(\frac{Q}{RT}\right) = A[\sinh(\alpha\sigma)]^n \quad . \qquad (2)$$

The parameters in Eq. (1) can be solved by using the nonlinear multivariate regression analysis with different strain rates and deformation temperatures at the true strain of 0.9. Constant α can be obtained by linear regression fit of σ - $\ln\dot{\varepsilon}$ and $\ln\sigma$ - $\ln\dot{\varepsilon}$. The average value of α at different strain rates is 0.0102. By taking the logarithm of Eq. (1), n and Q can be obtained. By plotting $\ln\dot{\varepsilon}$ and $\ln[\sinh(\alpha\sigma)]$, the slopes of the linear regression lines can be obtained, which correspond to n at different temperatures. Figure 4(a) shows the n values from 600 to 800 °C, which have an average value of 5.3 ± 0.3 except at 600 °C. By plotting $\ln[\sinh(\alpha\sigma)]$ and $1/T$, the slopes of the linear regression lines can be obtained, corresponding to Q/Rn at different temperatures. Figure 4(b) shows the deformation activation energy Q from 600 to 800 °C, which has an average value of 345 ± 9 kJ mol^{-1}.

Taking the logarithm of both sides of Eq. (2), the following relationship is obtained:

$$\ln Z = \ln A + n\ln[\sinh(\alpha\sigma)] \quad . \qquad (3)$$

By plotting $\ln Z$ and $\ln[\sinh(\alpha\sigma)]$, the intercept of the linear regression $\ln A$ can be obtained. The plot is shown in Fig. 4(c), where the intercept of the linear regression $\ln A$ is 37.81, giving the A value of 2.63×10^{16}. Then the constitutive equation that describes the flow stress, strain rate, and deformation temperature relationship can be represented as:

$$\dot{\varepsilon} = 2.63 \times 10^{16}[\sinh(0.0102\sigma)]^{5.3}\exp\left(-\frac{41500}{T}\right) \quad . \qquad (4)$$

Zeng et al.[22] determined an activation energy of 218–240 kJ mol^{-1} for hot deformation of bulk pure titanium, which is consistent with Frost and Ashby[23] 242 kJ mol^{-1} and Tanaka et al.[24] 240 kJ mol^{-1}. Their results are far from the activation energy of 345 kJ mol^{-1} obtained in this work from the powder compact forging process. The higher activation energy from our process is likely due to the occurrence of dynamic recrystallization during the hot deformation. Wanjara et al.[25] commented that the activation energy for processes controlled by a dynamic recrystallization mechanism is appreciably higher than those controlled by dynamic recovery. The deformation activation energy which is similar to the activation energy of self-diffusion is an indication of dynamic recovery, which is due to climb and cross-slip dislocation mechanisms.[26] The self-diffusion activation energy of titanium is 123 kJ mol^{-12}, which is much lower than the activation energy obtained from deformation in this work as 345 kJ mol^{-1}, indicating that the deformation mechanism of hot compression of CP Ti powder parts is dynamic recrystallization. The flow stress curves in Fig. 2 and microstructure in Fig. 3 for deforming CP Ti both confirmed that dynamic recrystallization occurs.

Another possible reason for the higher activation energy is the higher oxygen content in the sintered components which has a large influence on the titanium flow stress.[27,28] Oxygen (up to 0.3–0.5 wt%) works as an alloying element, which can induce high strength.[29] Wasz et al.[30] showed that the yield strength difference between Grade 1 (0.18 wt% O) and Grade 4 (0.40 wt% O) decreases from 400 MPa at room temperature to 50 MPa at 550 °C. Comparing our flow stress data in Fig. 2 with the data in Ref. 22, when titanium is compressed at 600 °C and 0.001^{-1}, the steady flow stress for the powder component is 140 MPa while for the bulk material it

https://doi.org/10.1557/jmr.2015.84 Published online by Cambridge University Press

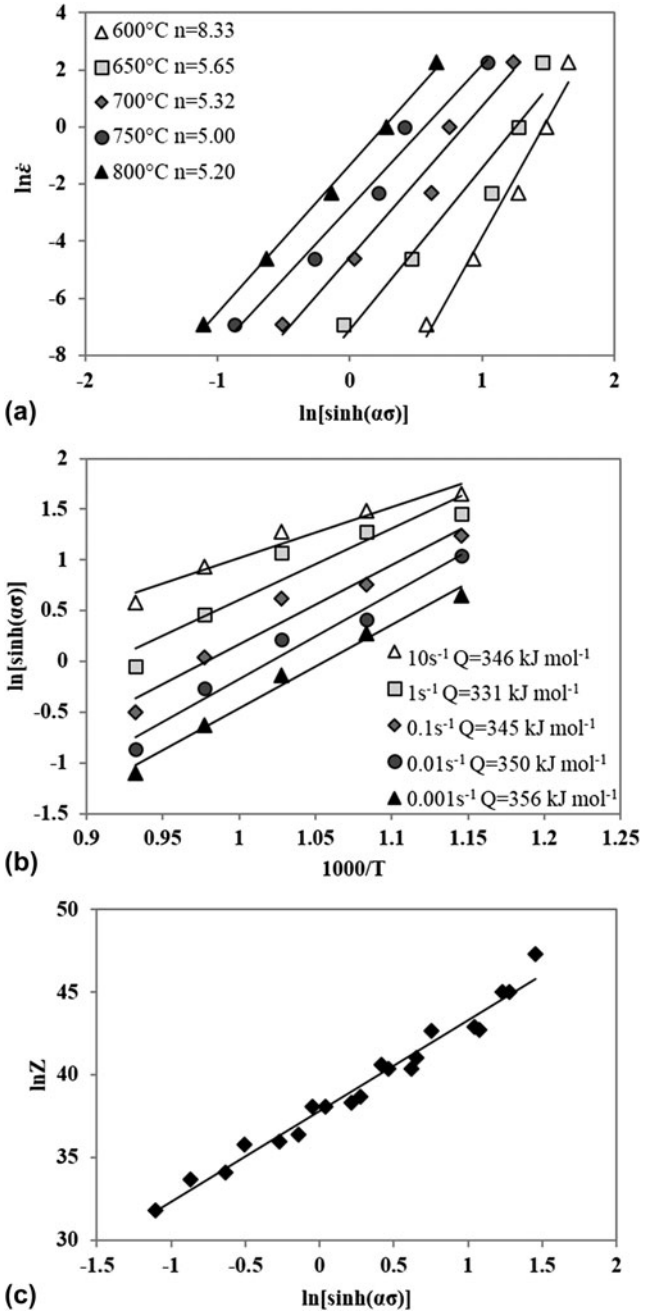


FIG. 4. (a) Relationship between stable flow stress and strain rate at different temperatures; (b) Relationship between stable flow stress and temperature at different strain rates; (c) Relationship between stable flow stress and Zener–Hollomon parameter.

is 80 MPa. However, when the deformation temperature increased to 700 °C, the difference between the flow stresses decreased to 15 MPa. From Eqs. (1) and (2), the flow stress has a proportional relationship with the deformation activation energy. This indicates that the flow stress difference of powder metallurgy and bulk CP Ti material reduced with increasing deformation temperature partially due to the different oxygen, which present similar phenomenon to Wasz et al.[30]

B. Processing map

The processing map consists of a superimposition of a power dissipation map and an instability map, which indicates the stable and unstable domain during the metal deformation. The dynamic material model developed by Prasad et al.[7] was used in this work. The unusual plastic and microstructural changes of the metal during hot deformation could indicate the power dissipation, which can be represented by the dimensionless parameter η (efficiency of power dissipation):

$$\eta = \frac{2m}{m+1} \quad , \tag{5}$$

Where m is the strain rate sensitivity, which is correlated with the flow stress and strain:

$$m = \frac{\partial \log \sigma}{\partial \log \dot{\varepsilon}} \quad . \tag{6}$$

The efficiency of power dissipation, deformation temperature, and strain rate form the power dissipation map, which indicates the behavior of how power dissipated under deformation.[31] Based on a microstructural change, Ziegler[32] proposes a dimensionless instability parameter $\xi(\dot{\varepsilon})$, which is defined as a function of strain rate and strain rate sensitivity:

$$\xi(\dot{\varepsilon}) = \frac{\partial \ln\left(\frac{m}{m+1}\right)}{\partial \ln(\dot{\varepsilon})} + m \quad . \tag{7}$$

$\xi(\dot{\varepsilon})$, strain rate, and deformation temperature form the instability map. The region where $\xi(\dot{\varepsilon})$ is negative indicates the microstructural instabilities of the material at the certain strain rate and deformation temperature. This work used the processing map generating procedure described by Prasad and Sasidhara in Ref. 33.

Figure 5 shows the processing map of hot deformed CP Ti powder compact at the true strain of 0.9 also with the microstructures at different regions. There are two blue regions on the top left and top right, which indicate the instability domain $\xi(\dot{\varepsilon})<0$. There are nine numbers, which represent different forging combinations (strain rate and deformation temperature) indicated on the processing map. The numbers correspond to nine groups of microstructure around the processing map. It can be seen in Fig. 5, when the material is deformed at 750 °C, different strain rates can lead to different microstructures. The 750 °C and 0.001 s^{-1} sample (⑧) provides a large grain size of 25 μm compared with the 750 °C and 10 s^{-1} sample (⑥) which has 10 μm grain size. The above two samples are fully dynamically recrystallized, however, for a strain rate value between these two, 0.1 s^{-1} (⑦), the microstructure shows partial recrystallization. The microstructure shows fine recrystallized grains along with the

https://doi.org/10.1557/jmr.2015.84 Published online by Cambridge University Press

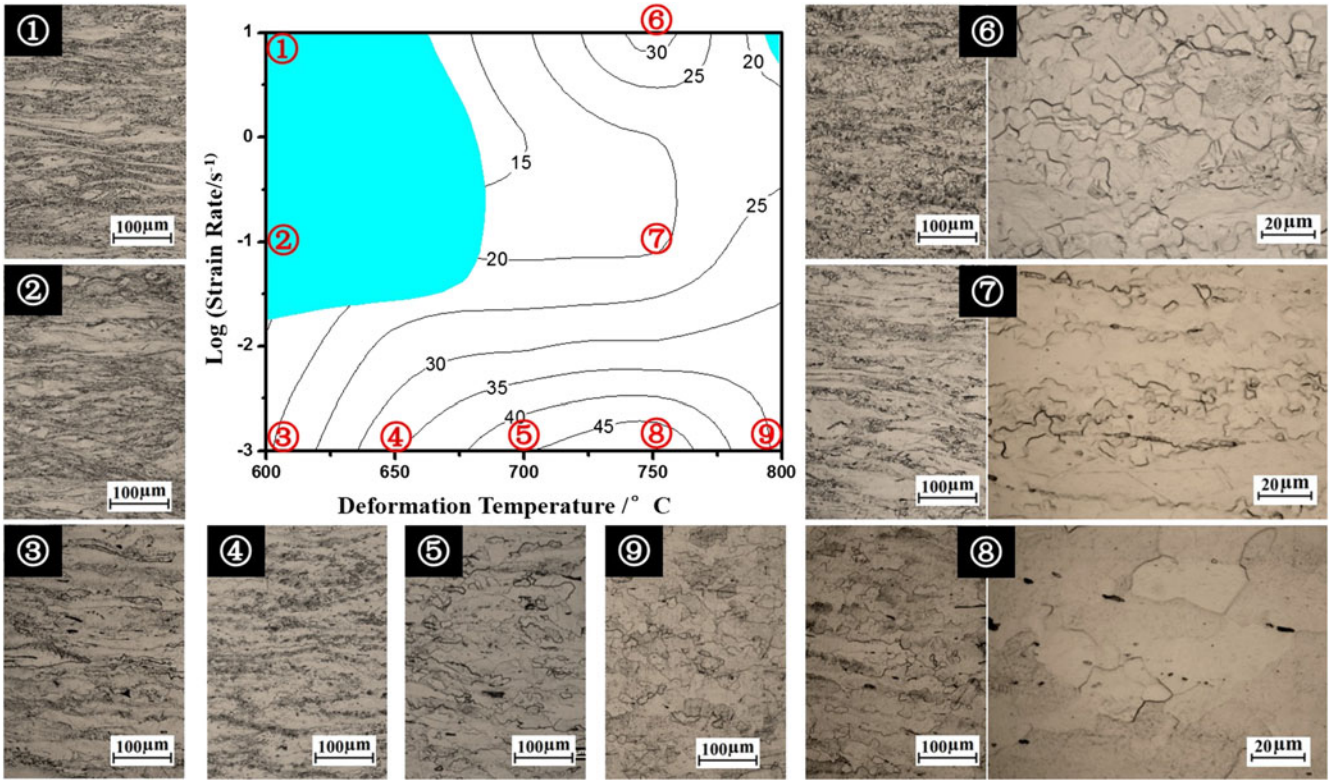


FIG. 5. Processing map from powder forging data at different true strains of 0.9 and the microstructures corresponding with the nine regions in the map. The numbers on the curves represent percent efficiency of power dissipation. The blue domains represent the unstable domains.

deformed nonrecrystallized grains, which corresponds to a lower efficiency of power dissipation (η = 20%) in region ⑦. The formation of the recrystallized nuclei on the interfaces has already occurred but the growth of these grains is slow. Regions ①, ②, and ③ are at different strain rates from 10, 0.1 to 0.001 s^{-1}, but at the same deformation temperature (600 °C). Regions ① and ② are the unstable domain, where the microstructure shows deformed grains and nucleated fine grains without growth, also the nucleation sites of the grains are highly nonuniform. Higher magnification microstructure of region ① shown in Fig. 3(a) indicates the heterogeneous microstructure. Regions ③, ④, ⑤, ⑧, and ⑨ are for the same strain rate (0.001 s^{-1}) but different deformation temperatures. From the microstructure in Fig. 5, with increase in the deformation temperature, the microstructure is more uniform with less unrecrystallized regions. That phenomenon is consistent with the processing map, with increasing deformation temperature, the efficiency of power dissipation is increased.

The processing map of bulk pure titanium has been studied by Prasad and Seshacharyulu[8] which contains 0.15 wt% oxygen from a temperature range of 600–850 °C. Both the bulk and powder titanium processing map show a trend that with decreasing temperature and increasing strain rate the power dissipation efficiency decreases. Also, the highest power dissipation efficiencies are both apparent in a region around 750 °C and 0.001 s^{-1} with a similar value of 45%. Thus the bulk and powder titanium deformation processing maps show a good agreement. However, there are several differences: Prasad and Seshacharyulu[8] obtain an unstable domain at the top region of the processing map, while the unstable domain is in the left top corner in this work; there is a low power dissipation efficiency region between 700–750 °C and 1–0.1 s^{-1} for deforming powder components. With a good consistency of the microstructure and power dissipation efficiency shown in Fig. 4, the 94% sintered density and 0.25% oxygen content processing map are convinced to be reasonable.

Furuhara et al.[34] revealed that subgrain boundaries (low-angle boundaries) form in the early stage of dynamic recovery of hot deformed Ti alloys by local orientation measurement. Chun and Hwang[35] showed that the warm deformation (60% reduction) of pure titanium under 450 °C produces well-defined subgrains and a virtually dislocation-free interior without initiation of recrystallization. But the 600 °C deformation temperature promotes the formation of high angle grain boundaries, and this causes the recrystallization nucleation to occur homogeneously. So the critical recrystallization temperature lies between 450 and 600 °C for 60% reduction bulk CP Ti. Recrystallized nuclei in our work show a volume fraction ranging from 10 to 70% at 600 °C

https://doi.org/10.1557/jmr.2015.84 Published online by Cambridge University Press

depending on different strain rates, which could indicate a start of dynamic recrystallization. The high deformation activation energy obtained from deforming CP Ti powder metallurgy, 345 kJ mol^{-1}, implies the dynamic recrystallization which agrees with his result. By increasing the deformation temperature, the orientation gradient increases, then nucleation of recrystallization is promoted.[35] This deduction is also well explained how deformation temperature affects the nucleation during forging CP Ti powder metallurgy parts in Fig. 5.

C. Density and microstructure transaction

Different with forging the bulk material, besides refining the microstructure due to the dynamic recrystallization, powder forging can also close the porosity remaining from the sintering process. Figure 6(a) shows the relative density obtained with image analysis. Most of the forged samples show a relative density from 98 to 99.9%. There is a trend that with increasing deformation temperature, the porosity in the observed domain decreased. However, the strain rate and porosity relationship under the same deformation temperature is not obvious. This phenomenon is correlated with the microstructure shown in Fig. 5 at 600 °C, the instability of the deformation might result in uneven closure of the pores.

Figure 6(b) shows the fully recrystallized grain size (750 and 800 °C) of the forged CP Ti compacts under different Z (Zener–Hollomon parameter) conditions. It can be seen that there is a clear trend that with increasing Z parameter (decreasing deformation temperature and increasing strain rate), the grain size is refined significantly from 25 to 10 μm. A high Z hot forging is useful for acquiring fine grains. Furuhara et al.[34] also revealed that high dynamic recrystallization of Ti alloys is effective in grain refinement when deformation is performed at a higher Z condition. Also, the necessary critical strain for complete dynamic recrystallization increases with increase of Z parameter.[36]

Figure 6(c) shows the contour map of the relationship of volume fraction of dynamic recrystallization, strain rate, and deformation temperature. The blue region at the right bottom of the map indicates the fully recrystallized domain, which temperature is higher than 700 °C and strain rate is lower than 0.01 s^{-1}. The low change recrystallized regions appear at lower temperature and strain rate. This contour map shows excellent agreement with the processing map in Fig. 5. This phenomenon indicates that the dynamic recrystallization of the deformed material has a direct correlation with the efficiency of power dissipation. This agreement verifies the accuracy of dynamic material model constructed by power dissipation efficiency from the microstructure observation point of view.

Power dissipation efficiency could be used to reflect the dynamic recrystallization in the stable domain.

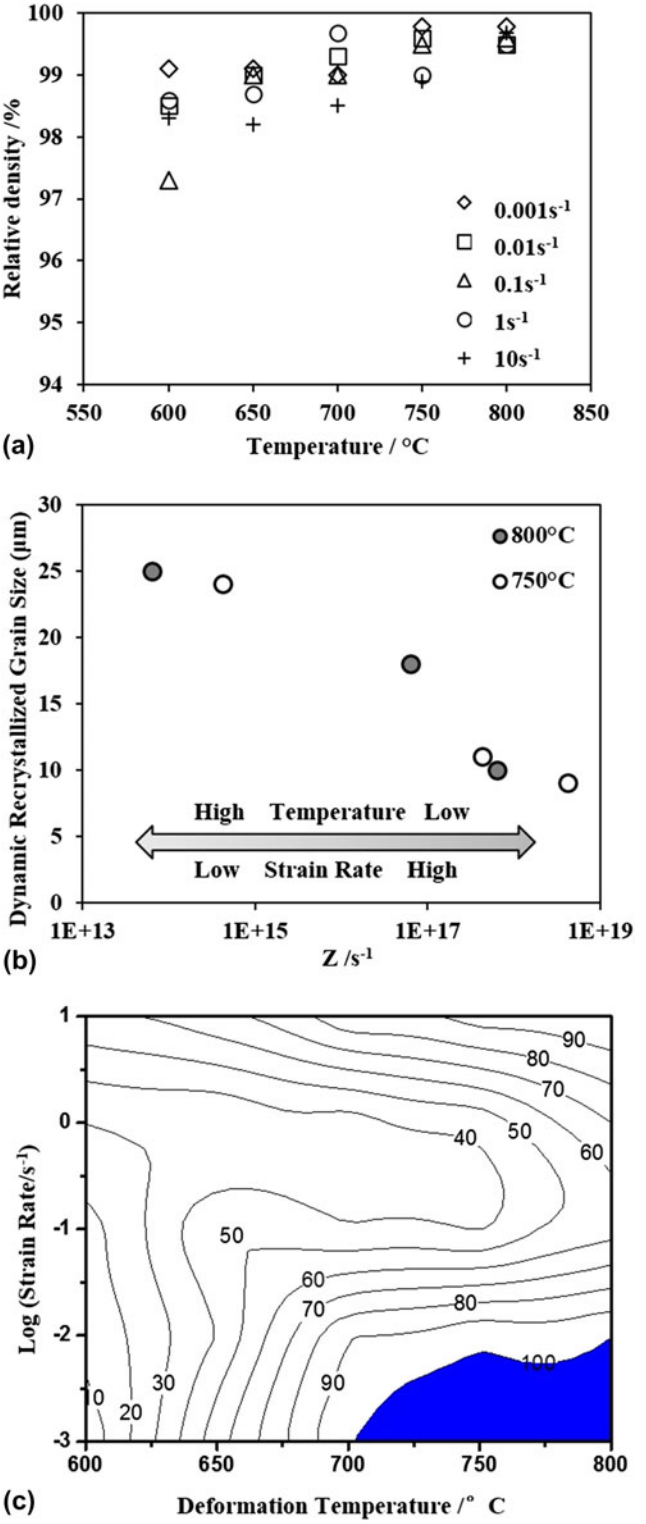


FIG. 6. (a) Relative densities of the CP titanium powder compact forging at different temperatures and strain rates; (b) Grain size of the forged recrystallized CP titanium powder compact at 750 °C and 800 °C with different Z parameters; (c) Volume fraction of recrystallization at different temperatures and strain rates.

Generally speaking, dynamic recrystallization takes place in the region which exhibits a power dissipation

https://doi.org/10.1557/jmr.2015.84 Published online by Cambridge University Press

efficiency from 30 to 55%, depending on the stacking fault energy.[9] For titanium alloy which has a higher stacking fault energy, dynamic recrystallization occurs at high values of power dissipation efficiency which is higher than 40%.[37] Also the high power dissipation value on the processing map could indicate superplasticity.[38] The stable region is in the area which has low strain rate and high power dissipation efficiency at 30–80% for Ti600 alloy.[9] For the 94% sintered density and 0.25% oxygen content powder component in this paper, when the power dissipation efficiency is higher than 40% (Fig. 5, regions ⑤, ⑧, and ⑨), complete dynamic recrystallization can be obtained as observed in the microstructure in Fig. 6(c). Although sample ⑦ was hot compressed at the same temperature with ⑥ and ⑧, the power dissipation efficiency (20%) is lower than ⑥(30%) and ⑧(45%), so the percentage of recrystallization is the lowest (40% recrystallization). Partial recrystallization occurs for power dissipation efficiency from 40 to 20%. The complete dynamic recrystallized region of powder metallurgy is consistent with the bulk titanium metals.

V. CONCLUSIONS

The consolidation and the flow behavior for forging powder compact CP titanium powder were studied and the following conclusions were listed:

(1) Hot powder forging can refine the grain size from 93 to 10 μm by the occurrence of dynamic recrystallization and also improve the densification of the powder metallurgy components to 99.9% when hot forging the 94% relative density powder compacts at 750 and 800 °C using a 10 s^{-1} strain rate.

(2) The relative density of the powder compact shows a proportional relationship with deformation temperature. The flow stress decreases with increasing deformation temperature, but the opposite with increasing strain rate.

(3) The constitutive equation for forging 94% titanium powder compact was determined with a deformation activation energy of 345 ± 9 kJ mol^{-1} and a strain hardening coefficient of 5.3.

(4) The processing map of the CP titanium powder compact is consistent with that for bulk titanium. Correlating with the volume fraction of the dynamic recrystallization obtained from microstructure analysis, when the power dissipation efficiency is higher than 40%, full dynamic recrystallization takes place. Partial recrystallization occurs for the power dissipation from 40 to 20%.

ACKNOWLEDGMENTS

We would like to acknowledge the financial support provided by Cristal Metal Inc. and Thermal Processing Technology Center in USA, the China Postdoctoral Science Foundation under Grant No. 2014M550235, and the Shanghai Postdoctoral Sustentation Fund under Grant No. 14R21410900.

REFERENCES

1. G. Lütjering and J.C. Williams: *Titanium* (Springer, Berlin, 2007).
2. R.M. German: *Sintering Theory and Practice* (Wiley, NewYork, USA, 1996).
3. X. Xu, G.L. Nash, and P. Nash: Sintering mechanisms of blended Ti-6Al-4V powder from diffusion path analysis. *J. Mater. Sci.* **49**, 994–1008 (2014).
4. Z. Zhang: Simulation of titanium and titanium alloy powder compact forging. Thesis, University of Waikato, Hamilton, New Zealand, 2011.
5. R.M. German: *Powder Metallurgy Science* (Metal Powder Industries Federation, Princeton, 1994).
6. R. Mythili, S. Saroja, and M. Vijayalakshmi: Study of mechanical behavior and deformation mechanism in an α–β Ti–4.4Ta–1.9Nb alloy. *Mater. Sci. Eng., A* **454–455**, 43–51 (2007).
7. Y.V.R.K. Prasad, H.L. Gegel, S.M. Doraivelu, J.C. Malas, J.T. Morgan, K.A. Lark, and D.R. Barker: Modeling of dynamic material behavior in hot deformation: Forging of Ti-6242. *Metall. Trans. A* **15**, 1883–1892 (1984).
8. Y.V.R.K. Prasad and T. Seshacharyulu: Processing maps for hot working of titanium alloys. *Mater. Sci. Eng., A* **243**, 82–88 (1998).
9. Y. Han, W. Zeng, Y. Qi, and Y. Zhao: Optimization of forging process parameters of Ti600 alloy by using processing map. *Mater. Sci. Eng., A* **529**, 393–400 (2011).
10. Z. Zeng, Y. Zhang, and S. Jonsson: Deformation behaviour of commercially pure titanium during simple hot compression. *Mater. Des.* **30**, 3105–3111 (2009).
11. W. Peng, W. Zeng, Q. Wang, and H. Yu: Comparative study on constitutive relationship of as-cast Ti60 titanium alloy during hot deformation based on Arrhenius-type and artificial neural network models. *Mater. Des.* **51**, 95–104 (2013).
12. X.G. Fan, H. Yang, and P.F. Gao: Prediction of constitutive behavior and microstructure evolution in hot deformation of TA15 titanium alloy. *Mater. Des.* **51**, 34–42 (2013).
13. A. Momeni and S.M. Abbasi: Effect of hot working on flow behavior of Ti-6Al-4V alloy in single phase and two phase regions. *Mater. Des.* **31**, 3599–3604 (2010).
14. X.Y. Zhang, M.Q. Li, H. Li, J. Luo, S.B. Su, and H. Wang: Deformation behavior in isothermal compression of the TC11 titanium alloy. *Mater. Des.* **31**, 2851–2857 (2010).
15. J. Jia, K. Zhang, and Z. Lu: Dynamic recrystallization kinetics of a powder metallurgy Ti-22Al-25Nb alloy during hot compression. *Mater. Sci. Eng., A* **607**, 630–639 (2014).
16. Metal Powder Industries Federation: *Standard Test Methods for Metal Powders and Powder Metallurgy Products* (Metal Powder Industries Federation, Princeton, 1985).
17. J. Svoboda and H. Riedel: Pore-boundary interactions and evolution equations for the porosity and the grain size during sintering. *Acta Metall. Mater.* **40**(11), 2829–2840 (1992).
18. S.L. Kang: *Sintering: Densification, Grain Growth & Microstructure* (Elsevier Butterworth-Heinemann, Burlington, UK, 2005).
19. X. Xu and P. Nash: Sintering mechanisms of Armstrong prealloyed Ti-6Al-4V powders. *Mater. Sci. Eng., A* **607**, 409–416 (2014).
20. C.M. Sellars and W.J. McTegart: On the mechanism of hot deformation. *Acta Metall.* **14**, 1136–1138 (1966).
21. C. Zener and J.H. Hollomon: Effect of strain rate upon plastic flow of steel. *J. Appl. Phys.* **15**, 22–32 (1944).

https://doi.org/10.1557/jmr.2015.84 Published online by Cambridge University Press

22. Z. Zeng, S. Jonsson, and Y. Zhang: Constitutive equations for pure titanium at elevated temperatures. *Mater. Sci. Eng., A* **505**, 116–119 (2009).
23. H.J. Frost and M.F. Ashby: *Deformation Mechanism Maps* (Pergamon Press, Oxford, 1982).
24. H. Tanaka, T. Yamada, E. Sato, and I. Jimbo: Distinguishing the ambient-temperature creep region in a deformation mechanism map of annealed CP-Ti. *Scr. Mater.* **54**, 121–124 (2006).
25. P. Wanjara, M. Jahazi, H. Monajati, S. Yue, and J-P. Immarigeon: Hot working behavior of near-α alloy IMI834. *Mater. Sci. Eng., A* **396**, 50–60 (2005).
26. T. Sheppard and J. Norley: Deformation characteristics of Ti-6Al-4V. *Mater. Sci. Technol.* **4**, 903–908 (1988).
27. J.C. Williams, A.W. Sommer, and P.P. Tung: The influence of oxygen concentration on the internal stress and dislocation arrangements in α titanium. *Metall. Trans.* **3**, 2979–2984 (1972).
28. I. Weiss and S.L. Semiatin: Thermomechanical processing of alpha titanium alloys—An overview. *Mater. Sci. Eng., A* **263**, 243–256 (1999).
29. I.I. Kornilov: Effect of oxygen on titanium and its alloys. *Met. Sci. Heat Treat.* **15**, 826–829 (1973).
30. M.L. Wasz, F.R. Brotzen, R.B. McLellan, and A.J. Griffin: Effect of oxygen and hydrogen on mechanical properties of commercial purity titanium. *Int. Mater. Rev.* **41**(1), 1–12 (1996).
31. S.V.S. Narayana Murty, B. Nageswara Rao, and B.P. Kashyap: Clarification on the physical dimension of K in a constitutive equation for superplastic flow: $\Sigma = K\varepsilon_m$. *J. Mater. Process. Technol.* **124**, 259 (2002).
32. H. Zeigler: Some extremum principles in irreversible thermodynamics with application to continuum mechanics. In *Progress in Solid Mechanics*, Vol. **4**, I.N. Sneedon and R. Hill eds. (Wiley, New York, 1963); p. 63.
33. Y.V.R.K. Prasad and S. Sasidhara: *Hot Working Guide: A Compendium of Processing Maps* (ASM International, Materials Park, OH, 1997); pp. 25–157.
34. T. Furuhara, B. Poorganji, H. Abe, and T. Maki: Dynamic recovery and recrystallization in titanium alloys by hot deformation. *JOM* **59**(1), 64–67 (2007).
35. Y.B. Chun and S.K. Hwang: Static recrystallization of warm-rolled pure Ti influenced by microstructural inhomogeneity. *Acta Metall.* **56**(3), 369–379 (2008).
36. S.V.S. Narayana Murty, S. Torizuka, and K. Nagai: Microstructural evolution during simple heavy warm compression of a low carbon steel: Development of a processing map. *Mater. Sci. Eng., A*, **410–411**, 319–323 (2005).
37. C. Poletti, H.P. Degischer, S. Kremmer, and W. Marketz: Processing maps of Ti662 unreinforced and reinforced with TiC particles according to dynamic models. *Mater. Sci. Eng., A* **486**, 127–137 (1998).
38. O.D. Sherby, R.D. Caiigiuri, E.S. Kayali, and R.A. White: Fundamentals of superplasticity and its applications. In *Advances in Metal Processing*, J.J. Burke, R. Mehrabian, and V. Weiss eds.; Plenum Press: New York, 1981; pp. 133–170.

https://doi.org/10.1557/jmr.2015.84 Published online by Cambridge University Press